# Fiber Bragg Grating Sensors-Based Assessment of Laser Ablation on Pancreas at 808 and 1064 nm Using a Diffusing Applicator: Experimental and Numerical Study

Pouya Namakshenas, Leonardo Bianchi, *Member, IEEE,*
and Paola Saccomandi, *Senior Member, IEEE*

Abstract—Laser ablation (LA) holds great promise for the localized treatment of pancreatic tumors. However, there are still many technical aspects that require improvements before largely applying this technique in clinical practice. This work shed light on the following subjects: the thermal response of the pancreas to LA using a diffusing applicator and delivering different laser wavelengths (i.e., 808 and 1064 nm); the development of a pancreas-specific numerical model with temperature-dependent tissue properties based on non-Fourier heat conduction for predicting the temperature distribution. To experimentally study the pancreas thermal response and to tune the model parameters, 80 fiber Bragg grating (FBG) sensors, embedded in arrays with millimetric spatial resolution, were implanted in ex vivo pancreas undergoing LA to obtain the real-time and 2-D temperature distribution. Based on the temperature measured by the FBG sensors, results show that the laser wavelength affects the pancreas thermal response: at 2 mm from the applicator, LA at 808 nm resulted in a thermally affected area 5%–15% larger than at 1064 nm, whereas no notable difference was observed at 6 mm. The temperature distribution and laser-induced lesion obtained from the non-Fourier numerical model were found to closely match the experimental results when the phase lag of the temperature gradient was five times that of the heat flux vector.

Index Terms—Diffusing applicator, fiber Bragg grating (FBG), laser ablation (LA), mathematical modeling, pancreas, temperature monitoring.
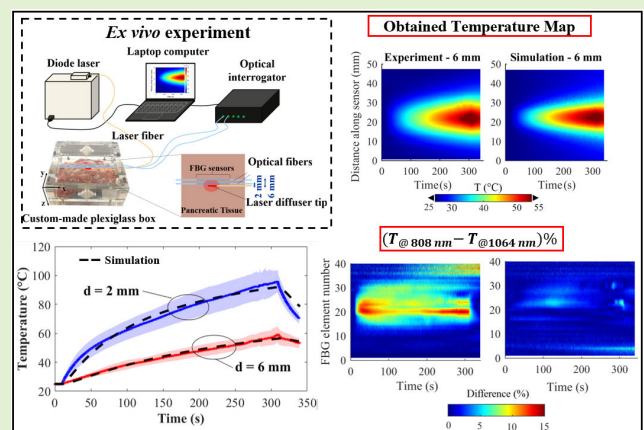
I. INTRODUCTION

PANCREATIC cancer ranked third among cancer deaths in the United States in 2022, according to the American Cancer Society statistics. Data from people who were diagnosed with pancreatic cancer between 2011 and 2017 show that the five-year relative survival rate is around 11% for all stages, including localized, regional, and distant cancer [1]. More

than 90% of pancreatic cancers are adenocarcinoma type, which rarely shows symptoms until they are advanced, making surgery an impractical option [2]. Other treatment modalities, such as chemotherapy and radiotherapy, do not also meet the treatment outcome criteria for most cases of pancreatic cancer. Considering the statistics, finding effective treatment strategies for this type of cancer is imperative. Modern approaches, including locoregional ablation, have shown significant potential for the treatment of several tumors, and pancreatic cancer can benefit from these techniques [3], [4]. Indeed, thermotherapy can be effective in the treatment of inoperable patients, as, in tumors like hepatocellular carcinoma, thermotherapy has demonstrated the same efficacy as surgery. The main benefits of thermotherapy are associated with reduced invasiveness and pain, resulting in shortened hospital stays and a consequent increase in life quality. For unresectable tumors at critical sites (like in the pancreas), laser ablation (LA) is the desirable thermotherapy technique, as it employs a thin and flexible

light-guiding fiber enabling minimally invasive treatment, thus minimizing the impact on the surrounding anatomical structures. Recent clinical trials have confirmed LA's potential in treating pancreatic ductal adenocarcinoma [5], [6]. LA causes thermo-coagulation of cancerous tissue by exploiting the interaction between laser light and tissue. The photons emitted by a monochromatic, coherent, and collimated laser source are scattered and absorbed by the tissue, and this energy is then converted into heat. The laser wavelength is the primary determinant of absorption: for achieving the desired thermal effect, it is important to select a laser working in the so-called "therapeutic window," which comprises near-infrared (NIR) wavelengths (NIR I, which includes 808 nm, and NIR II, which includes 1064 nm).

Until now, LA of pancreatic tumors has been executed with bare fiber applicators [5], [6], but the diffusing ones may offer more benefits due to the reduced power density [7], [8]. Besides, diffusing applicators can provide a more extended ablation volume than bare-type applicators, making them a better choice, especially for the removal of large tumors. Using a bare fiber applicator, Di Matteo et al. [9] performed ex vivo LA on porcine pancreases using a laser energy level of 1000 J (power range 1.5–20 W). They observed that the ablation volume saturates after 10 W, and it may be a consequence of carbonization. Truong et al. [7] conducted LA under the same condition as Di Matteo et al. [9], but with a diffusing applicator. No carbonization was observed, and a linear relationship existed between the laser power and the ablation volume. Considering in vivo studies of Lim et al. [10] on LA with diffusing applicator on mini-pigs, no thermal damage to the surrounding sensitive structures, such as vessels, was reported [7], [10]. Despite the impressive potential of the diffusing applicator, only a few studies are available on laser-pancreatic tissue interaction; there is no evaluation of the effect of laser wavelength, and limited information on the resulting temperature distribution is available [7], [10], [11].

Having a strategy for intraoperative LA monitoring is a crucial aspect to assess the performance of the ablative technique and to guarantee a safe treatment. Several studies report temperature measurement approaches that have some limitations: for instance, the single-point tissue temperature time-history measurements, which do not provide a comprehensive picture of the tissue thermal response [12]; the use of infrared thermal cameras, which are suitable only for superficial measurements, whereas in most cases, the laser applicator is located deep inside the tissue [7].

A solution to this need is solved by using temperature sensors based on fiber Bragg grating (FBG). Relying on the wavelength-division multiplexing capability, FBGs allow measuring the tissue temperature distribution on tens of locations with a millimetric spatial resolution and high signal-to-noise ratio [13]. Other characteristics, such as the small size, immunity to electromagnetic fields, biocompatibility, and inertness, make FBG suitable for thermometry during thermal ablation procedures and for performing temperature-based LA control [13], [14]. The latest writing technology based on the femtosecond laser inscription allows high customization of the gratings and array features, thus optimizing the spatial resolution and the sensing length, which can reach submillimetric scale [13], [15].

Along with the strategy for intraoperative monitoring, also having a numerical and pancreas-specific tool to predict the temperature distribution at different laser settings is essential for optimizing the treatment toward its clinical application. Most previous studies rely on Fourier's law as the body of the heat transfer model. However, it was shown that there is a time delay for the thermal energy transport within biological tissues, especially when high heat flux is applied for a short amount of time [16], [17]. Therefore, the numerical analysis must be improved by incorporating this effect to predict the temperature distribution in the pancreas more accurately. Prior studies on LA in pancreas have simplified another key aspect: the optical and thermal properties used in the computational modeling did not correspond to the properties of the pancreas tissue. These approximations affect the prediction of temperature distribution, thus impairing the LA optimization for pancreas tumor treatment.

Based on all the lacking aspects outlined above in the field LA in pancreas, this study addresses the following open questions: 1) the accurate analysis of the thermal effects of a laser diffusing applicator; 2) the effect of the laser wavelength (i.e., 808 and 1064 nm) on the pancreas thermal response; and 3) the development of a pancreas-specific numerical tool with temperature-dependent tissue properties and based on non-Fourier heat conduction model for temperature distribution prediction. A network of quasi-distributed FBGs with millimetric spatial resolution has been used to investigate the three aspects above, including the estimation of the temperature gradient phase lag parameter for the pancreas.

II. MATERIALS AND METHODS

A. Laser Irradiation of Ex Vivo Pancreatic Tissues

NIR laser irradiation experiments were executed on ex vivo pancreatic tissue samples. Freshly excised healthy porcine pancreases were procured from a local slaughterhouse. The organs were first put in a sealed bag, transported to the laboratory inside an isolated ice-water-cooled container, and then stored in the refrigerator (i.e., at a temperature of 4 °C). Before irradiation, pancreases were removed from the refrigerator to achieve room temperature. Hence, tissue samples were cut from the entire organs to fit a custom-made plexiglass box. The box, manufactured with holes at specific distances, allowed the proper alignment and positioning of the temperature monitoring sensors and the laser-delivering applicator within the tissue (see Fig. 1). Two diode lasers (LuOcean Mini 4, *Lumics*, Berlin, Germany) both operating in the continuous-wave mode and emitting laser light at wavelengths within the NIR range (i.e., 808 and 1064 nm, respectively) were employed. The wavelengths of 808 and 1064 nm were chosen since they lie in the regions of the spectrum characterized by the lowest attenuation, hence the highest penetration depth, in pancreatic tissue [18]. To experimentally evaluate the thermal effects due to the laser–tissue interaction at the different wavelengths and allow for a comparison of the results, we irradiated the pancreas tissue samples either at 808 or 1064 nm at the same settings, i.e., laser power of 5 W and exposure time of 300 s
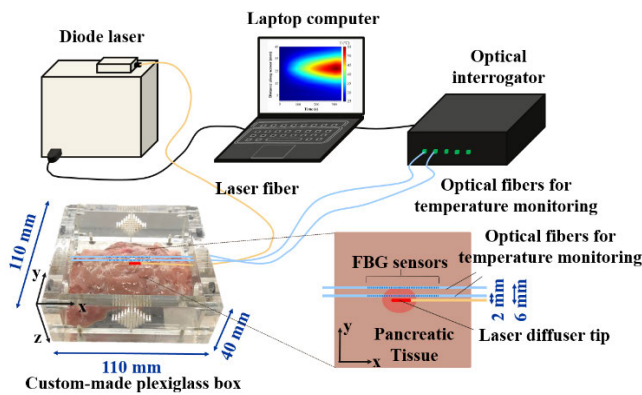
Fig. 1. Experimental setup utilized to perform laser irradiation of ex vivo porcine pancreatic tissues. The tissue samples were positioned in a custom-made plexiglass box. Diode lasers were used to irradiate the tissue samples (either at 808 or 1064 nm) through a cylindrical diffusing applicator; two optical fibers, each embedding 40 FBG sensors, connected to an optical interrogation unit, were employed to monitor the tissue temperature variation. The close-up (bottom right) shows the arrangement of the optical fibers for temperature monitoring and the laser diffuser tip.

(typical clinical settings). For each laser wavelength, three irradiation tests were repeated. The laser light was conveyed to the tissue by flexible fused silica optical fiber [low-OH core: 300 μm diameter, doped silica cladding: 330 μm diameter, and polyimide buffer: 370 μm diameter; numerical aperture (NA): 0.22]. Overall, the inner and outer diameters of the glass cap were 400 and 1000 μm, respectively. The fiber was coupled with the laser emitter at the proximal end and had a cylindrical diffuser tip at the distal extremity (*Polymicro, Molex*, Phoenix, USA). The cylindrical diffuser tip allowed a 360° circumferential light emission in the tissue. The threaded diffuser length was 10 mm, while the diffuser glass capillary was 17 mm.

B. FBG-Based Temperature Measurement and Experimental Arrangement

Fiber optic sensors are largely employed for healthcare purposes [19], [20]. In this study, FBG sensors were used to monitor the tissue temperature variation during experiments. The principle that stands at the basis of FBG-thermometry during thermal procedures is the detection of the Bragg wavelength shift in the FBG reflected spectrum due to the tissue temperature change. Hence, the tissue temperature variation can be indirectly measured by peak tracking FBG reflected spectrum [15], [21]. An industrial optical sensing interrogator (Micrometer Optics si255 optical interrogator, Micrometer Optics Inc., Atlanta, USA, 1 P.M. accuracy corresponding to 0.1 °C, 1460–1620-nm wavelength range), with a 100-Hz sampling rate, was utilized to illuminate the FBG sensors and acquire the reflected spectra. The optical data were sent to a computer, so that the tissue temperature values were visualized in real time, as well as registered for postprocessing, by means of a custom LabVIEW program (see Fig. 1). In our setup, we employed two polyimide-coated single-mode optical fibers SM1500(9/125)P (Fibercore, Ltd., Southampton, U.K.), in which the FBG arrays were inscribed with femtosecond

point-by-point writing technology [22]. Each fiber had an array of 40 FBG sensors, characterized by an edge-to-edge distance between consecutive gratings of 0.01 mm and a grating length of 1.19 mm. Hence, the total sensing length per fiber was 48 mm (spatial resolution equal to 1.2 mm). A total of 80 sensors was used to measure the temperature map in the pancreas. The FBGs were uniformly distributed in the 1460–1620-nm wavelength range (spectral range of the interrogation unit), and each single resonance peak of the FBG array was characterized by a narrow spectral width in order to minimize the influence of surrounding resonances upon heating. The value of the thermal sensitivity of the sensors was $(7.43 \pm 0.01) \times 10^{-6}$ °C^{-1}. The properties of the coating material (i.e., polyimide) of the fibers, e.g., low thermal conductivity and high thermal resistance [22], [23], and the array characteristics were advantageous for resisting high temperature and accurately detecting high-temperature gradients through quasi-distributed sensing. Indeed, during LA, there exists the possibility of reaching high temperatures and high thermal gradients (e.g., 50 °C/mm), especially close to the applicator tip [24].

For accurate positioning, a slab of tissue was inserted into the box, the laser applicator was inserted through the central hole of the lateral face of the box, and two metallic needles (21 gauge) were inserted at the distances of 2 and 6 mm from the applicator insertion, parallel to the laser applicator. The optical sensing fibers were then inserted into the needles. Afterward, the metallic needles were removed, leaving the optical sensing fibers on the tissue at the selected distances from the diffusing laser applicator. A second slab of the same tissue sample was then positioned on the first one, so that the laser applicator fiber and the optical fibers for temperature measurement were interstitially positioned in the tissue.

For each test, the initial temperature of the tissue (25 °C) was measured with a k-type thermocouple (0.1 °C accuracy). Then, the temperature variation in tissue was monitored by the FBG sensors for 10 s before laser irradiation, then, during laser irradiation (300 s), and, finally, for 30 s after irradiation (cooling process). Temperature measurement results are presented as mean value $\pm$ standard deviation, calculated on the three repeated tests at the same experimental conditions (i.e., laser wavelength and power).

C. Numerical Model Based on Dual-Phase Lag (DPL)

Previous studies have demonstrated that in biological tissues with nonhomogeneous inner structures, there is a relaxation mechanism that delays the response between the heat flux vector and the temperature gradient [25]. To address this issue, non-Fourier models like hyperbolic thermal wave and DPL models have been proposed. Theoretically, the exchange between heat flux and temperature gradient in nonhomogeneous materials, such as biological tissues, takes seconds. To consider the effect of tissue microstructure on heat transfer, the thermal behavior of pancreatic tissue was modeled by the non-Fourier-based DPL model incorporating the heat flux phase lag (τ_q), also called thermal relaxation time, and the

temperature gradient phase lag (τ_T) as follows [26], [27]:

$$\nabla\left[k\nabla\left(T + \tau_T\frac{\partial T}{\partial t}\right)\right]$$
$$= \left(1 + \tau_q\frac{\partial}{\partial t}\right)\left(C_v\frac{\partial T}{\partial t} + \omega_b C_{v,b}\,(T - T_b)\right.$$
$$\left. - Q_{\text{met}} + Q_{\text{ev}} - Q_L\right) \quad (1)$$

$$Q_{\text{ev}} = -h_{\text{fg}}\left(\frac{\mathrm{d}W(T)}{\mathrm{d}t}\right). \quad (2)$$

A limited number of values have been reported for the thermal relaxation time of biological tissues, including 16 s [28] and 1.77 s [29] for processed meat, 1.17 s for ex vivo sheep lung [30], and 5.66 s for ex vivo bovine liver [31]. Currently, no data are available for the phase lag attributed to the heat flux in pancreatic tissue, so we based this value on the measurements of the bovine liver [31]. Taking τ_q as a given, we considered various τ_T values as a ratio of τ_q to determine a tolerable error between ex vivo measurements and DPL predictions. The Pennes model can be regenerated by substituting zero for phase lags in (1). Since the experiments were performed under the ex vivo condition, the blood perfusion rate ω_b (1/s) and the metabolic heat of the tissue Q_{met} (W/m³) were considered to be zero in the model. The term of heat loss due to the tissue water evaporation Q_{ev} (W/m³) can be modeled by (2), where $h_{\text{fg}} = 2260$ kJ/kg is the latent heat of water and $W(T)$ is the water content ratio remaining in the tissue as a function of temperature during LA and its change was taken into account by the equations described in [32] and [33]. The radial laser heat source Q_L (W/m³) was described by a diffusion approximation according to the Beer–Lambert law as follows:

$$Q_L = \mu_{\text{eff}} \cdot \left(\frac{P}{2\pi r l}\right)\exp(-\mu_{\text{eff}} \cdot r) \quad (3)$$
$$\mu_{\text{eff}} = \sqrt{3\alpha(\alpha + \alpha'_s)} \quad (4)$$
$$\alpha'_s = \alpha_s\,(1 - g) \quad (5)$$

where $\mu_{\text{eff}}(\text{cm}^{-1})$ is the effective attenuation coefficient, $P(\text{W})$ is the laser power, $r(\text{cm})$ is the radial distance from the applicator, and $l(\text{cm})$ is the active length of the applicator. As per (4), the effective attenuation coefficient $\mu_{\text{eff}}(\text{cm}^{-1})$ is a lumped property that describes the light's absorption and scattering phenomena inside the tissue. The reduced scattering coefficient, denoted as $\alpha'_s(\text{cm}^{-1})$ in (4), is a function of scattering coefficient $\alpha_s(\text{cm}^{-1})$ and the anisotropy factor g, as described in (5). The thermal and optical parameters are presented in Table I. The thermal–physical properties of pancreatic tissue used in the model have been previously measured by the same research group [18], [34]. In particular, the model includes temperature-dependent thermal properties and optical properties measured in a broad spectral range. Equations (1)–(5) were implemented in COMSOL Multiphysics (COMSOL, Inc., Burlington, MA, USA), a finite element method-based software under a 2-D axial symmetric setting. The generalized alpha transient solver was utilized to solve the DPL model.

TABLE I
THERMAL AND OPTICAL PARAMETERS USED IN THE NUMERICAL MODEL

Parameter	Definition	Pancreas	Glass	Air
$k_{25\,°C}$ [(1)]	Thermal conductivity, $W/(m \cdot K)$	0.52 [34]	1.3 [12]	0.026 [12]
$C_{v,25\,°C}$ [(1)]	Volumetric heat capacity, $MJ/(m^3 \cdot K)$	3.72 [34]	1.802 [12]	0.001 [12]
τ_q	Heat flux time delay, s	5.66 [31]		
τ_T	Temperature gradient time delay, s	1.13 - 28.30		
α	Absorption coefficient, $1/cm$	0.116@808nm, 0.168@1064nm [18]		
α'_s	Reduced scattering coefficient, $1/cm$	17.423@808nm, 12.621@1064 [18]		

[(1)] The parameter's value at the beginning of experiments (T = 25 °C). The model takes into account the temperature-dependent parameter value of the pancreatic tissue from our previous measurements [34].

III. RESULTS AND DISCUSSION

This section presents the results in a structure that follows. First, we compare the temporal temperature profiles derived from different implemented models with the experimental data in order to find the closest fit. For further evaluation, the spatiotemporal temperature maps along the FBG arrays and the ablation zone defined by 60 °C are compared to the best model. The last part compares the thermal effects of LA based on temperature records taken from the experiments at the two selected wavelengths.

A. Selecting the Best-Fit Theoretical Model

In Fig. 2, the results of the Pennes model and the DPL model at different phase lag ratios ($\tau_T = 1/5\tau_q$, $\tau_T = 1/2\tau_q$, $\tau_T = \tau_q$, $\tau_T = 2\tau_q$, and $\tau_T = 5\tau_q$) are compared to ex vivo experiments based on the profile of the maximum temperature at wavelengths of 808 and 1064 nm and at two different distances of 2 and 6 mm. The main difference between models appears during the irradiation time and at closer distances from the applicator, such as 2 mm. For example, at 808 nm, the Pennes model predicts 8.5 °C and 3 °C higher temperatures than the experiments in the middle of irradiation ($t = 150$ s), whereas the DPL model ($\tau_T = 5\tau_q$) predicts 3 °C and 1 °C deviation. Due to the Fourier assumption behind Pennes model, the former predicts higher temperatures during irradiation, while the DPL model predicts smoother temperature rises more in line with the experimental trends. Generally, in the DPL model, a lower temperature gradient is associated with a higher ratio between temperature phase lag (τ_T) and heat flux phase lag (τ_q). Among the set ratios, when $\tau_T = 5\tau_q$, the temperature profiles approach those of the experiments during the irradiation. A maximum deviation of ~12% and ~14% takes place at 2 mm between the DPL model ($\tau_T = 5\tau_q$) and the experiments at 808 and 1064 nm, respectively. It should be noted that the temperature values of the Pennes model are closer to the experiments during the cooling period; however, there is a small deviation between
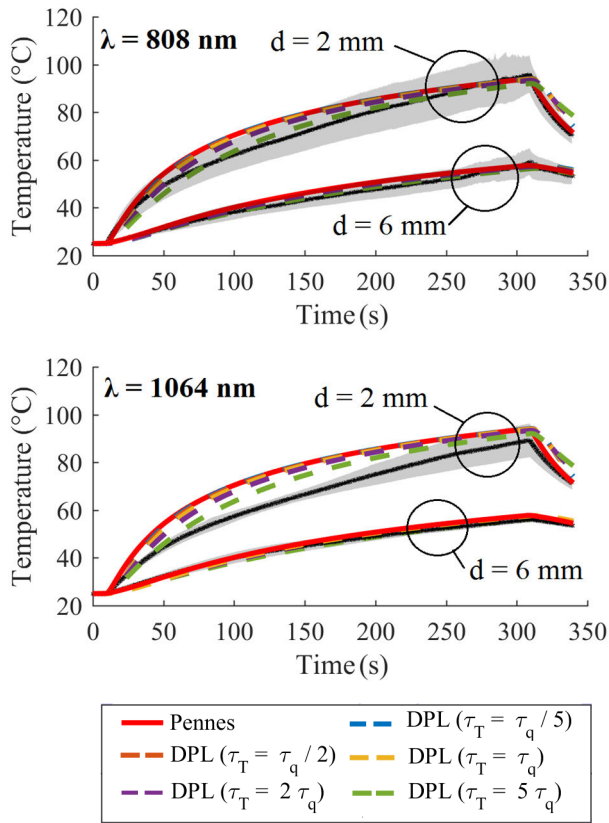
Fig. 2. Comparison of the maximum temperature values between theoretical models and ex vivo experiments at distances of 2 and 6 mm from the applicator to find the best-fit relationship between phase lag values. Based on three repeated experiments in each group, solid black lines display the average results, and gray areas display the standard deviation.

all the models in the cooling. Both the theoretical models and experimental results show that the temperature decreases more rapidly at a distance of 2 mm compared to 6 mm during the cooling process. Temperature profiles from the studied models converge at the end of irradiation, similar to the trend in [31].

B. Evaluating the Best-Fit Model Using Experimental Temperature Maps

Temporal temperature distributions based on the DPL model ($\tau_T = 5\tau_q$) along two paths equal in length to the sensing part, at 2 and 6 mm, are compared with those recorded in ex vivo experiments on the FBGs during the LA by 808 nm [see Fig. 3(a)] and 1064 nm [see Fig. 4(a)] wavelengths. In spite of the good agreement between the present model and experiments in terms of temperature rise, the simulation shows a narrower thermally affected area, which can be attributed to the simplification of the laser diffusive pattern made in our simulation, i.e., in the position of 2 mm at 808 nm, the length of optical fiber undergoing the temperature higher than 50 °C is 0.5 mm ($t = 100$ s), 2.5 mm ($t = 200$ s), and 3.5 mm ($t = 300$ s) more than the simulation. The discrepancy at 2 mm can possibly be due to changes in tissue properties close to the laser applicator. Simulations are more consistent with experiments at 6 mm compared to 2 mm, i.e., in the position of 6 mm at 808 nm; similar to the simulation results, the optical
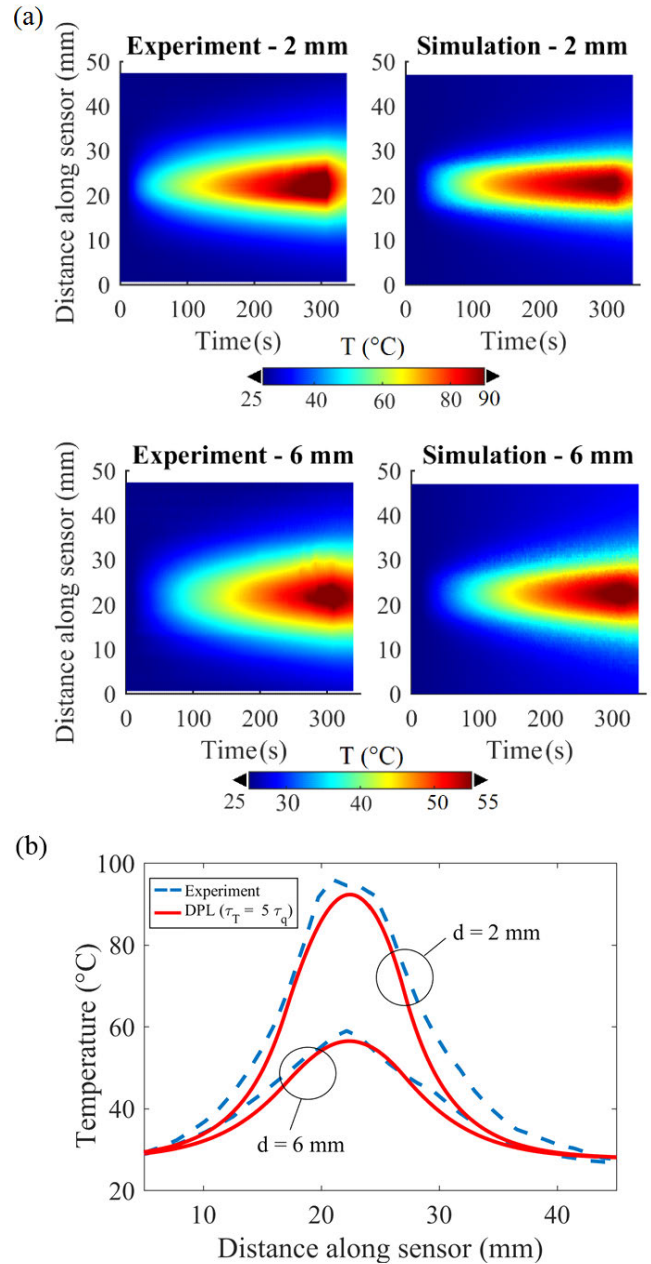

Fig. 3. Evaluation of the DPL model's predictions when $\tau_T = 5\tau_q$ through ex vivo experiments conducted at a wavelength of 808 nm. (a) Time history of the temperature records along the sensors. (b) Spatial temperature profiles at 310 s captured at 2- and 6-mm distances from the laser applicator. The experimental data visualization is based on the average of three repeats in each group.

fiber senses 50 °C after 200 s, and the length of optical fiber undergoes this threshold is 0.5 mm ($t = 250$ s) and 0.5 mm ($t = 300$ s) more than the simulation. The clinicians usually consider a 5 mm of safety margin around the tumor during the LA operation; hence, the maximum difference between the simulation and experiments in the thermally affected area is acceptable since it is less than the confidence interval [35]. Spatial temperature profiles along the sensor at the end of irradiation ($t = 310$ s) are also compared with the DPL model prediction made at 808-nm [see Fig. 3(b)] and 1064-nm [see Fig. 4(b)] wavelengths.
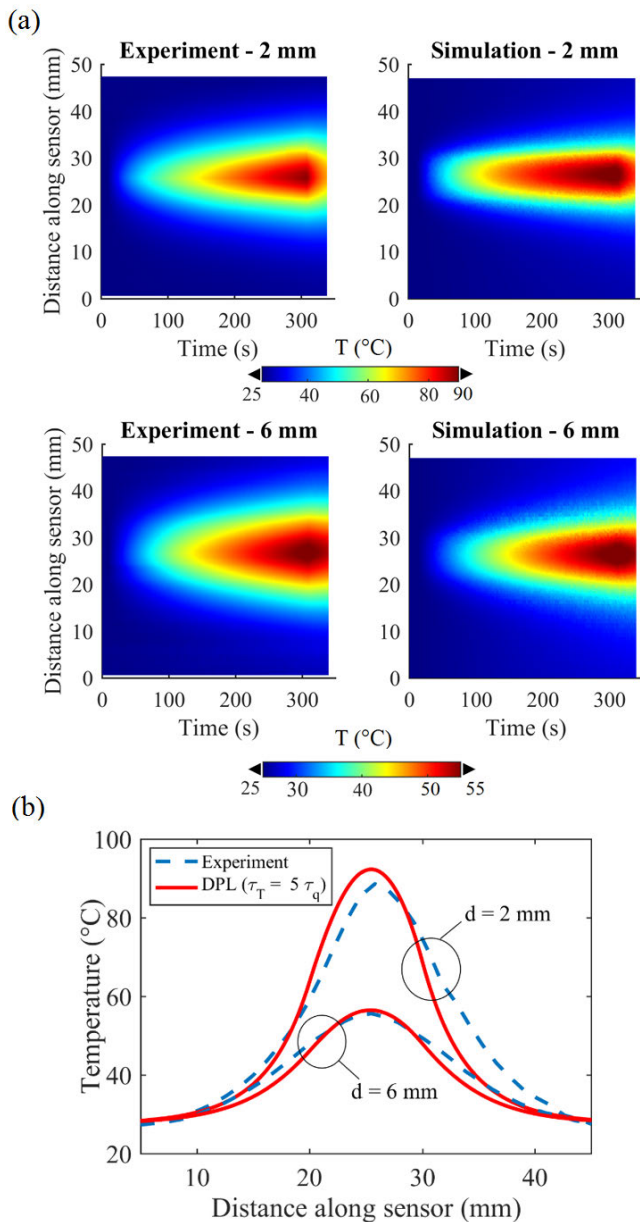
(a)

(b)

Fig. 4. Evaluation of the DPL model's predictions when $\tau_T = 5\tau_q$ through ex vivo experiments conducted at a wavelength of 1064 nm. (a) time history of the temperature records along the sensors. (b) Spatial temperature profiles at 310 s captured at 2- and 6-mm distances from the laser applicator. The experimental data visualization is based on the average of three repeats in each group.

As an important part of the LA efficacy, the extent of the ablation zone should be planned. In Fig. 5, the ablation zone is defined by the temperature threshold of $T = 60\ °C$ [36], [37]. Fig. 5(a) shows a comparison between the Pennes and DPL models ($\tau_T = 5\tau_q$) prediction and those observed in ex vivo experiments at 2-mm intervals, since in Figs. 3 and 4, the maximum temperature at 6 mm intervals does not exceed $60\ °C$. The Pennes model predicts ablation much earlier than the experiments, but the DPL model is closer to the experiments because it takes into account the time delays caused by the thermal inertia and tissue microstructure heterogeneity. Comparing the enclosed areas in Fig. 5(a), which represent the
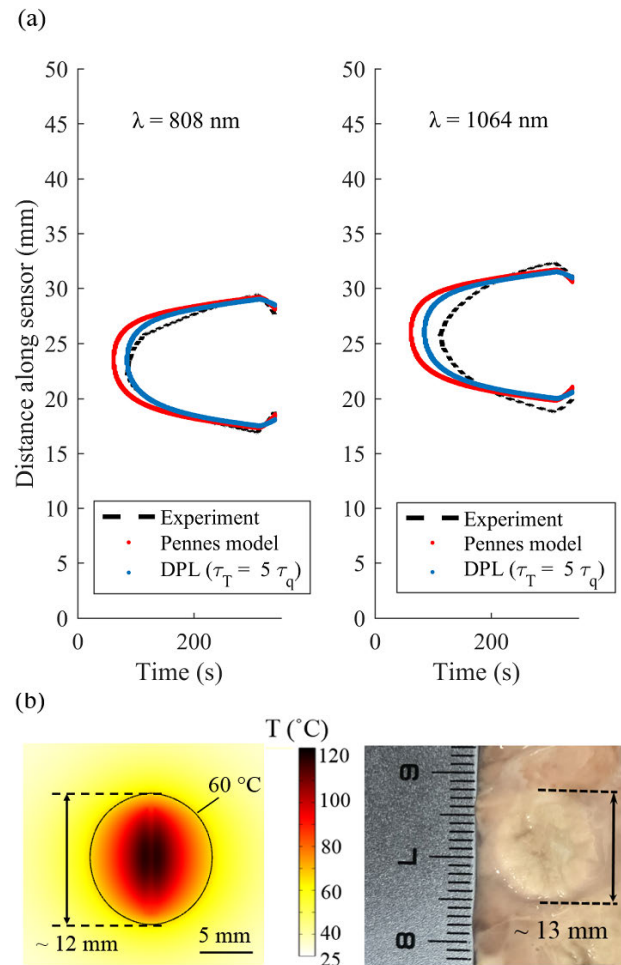
(a)

(b)

Fig. 5. Comparison of the Pennes and the DPL ($\tau_T = 5\tau_q$) models with ex vivo experiments in terms of the ablation zone evolution with an indicator of $T = 60\ °C$ (a) captured by FBGs at 2 mm for wavelengths of 808 and 1064 nm and (b) appearing on the pancreas for one of the tests by 1064 nm.

evolution of the ablation zone along the optical fiber, differs by 13% (808 nm) and 16% (1064 nm) according to the Pennes model and by 2% (808 nm) and 7% (1064 nm) according to the DPL model. While the DPL prediction and experiments are in good agreement, there is a discrepancy that can be explained by the variability of optical properties in pancreatic tissue, i.e., the reduced scattering coefficient of fresh ex vivo porcine pancreatic tissue ranges between ∼10.1 and 24.8 cm^{-1} at 808 nm, whereas at 1064 nm, they range between ∼6.5 and 18.7 cm^{-1}. Fig. 5(b) illustrates the size of the ablation zone that appeared on the tissue after an experiment conducted at 1064 nm and the predicted result based on the DPL model. The model and experiment agree well since both exhibit circumferential ablation with a difference of 1 mm in both axes.

C. Comparison of the Temperature Distribution at 808 and 1064 nm

In this section, we compare the LA thermal outcome on the pancreatic tissue at 808- and 1064-nm wavelengths. Fig. 6 shows the temperature records of 40 FBGs during the LA at
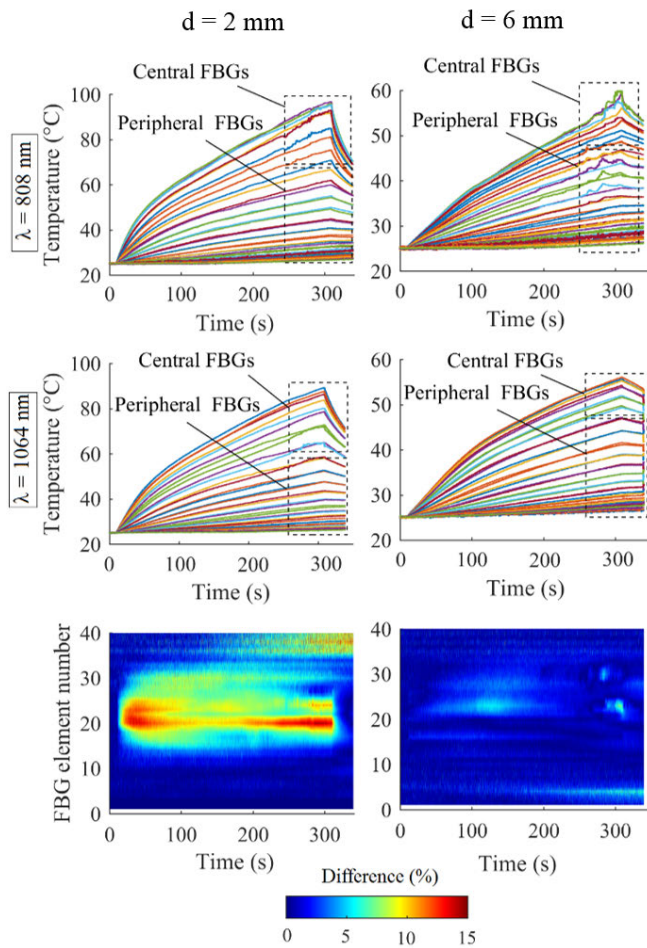
Fig. 6. Temperature distribution recorded by two chains of 40 FBG sensors at 2 and 6 mm of the laser applicator induced by wavelengths 808 and 1064 nm. Defined central FBGs correspond to the sensing length with which the diffusing length is covered, and peripheral FBGs measure the temperature of tissues nearby the irradiated area. 2-D maps show the difference in temperature distribution between the two wavelengths. The data visualization is based on the average of three repeated tests per wavelength.

808 and 1064 nm and illustrates the differences in temperature distribution at those wavelengths on each sensor. Based on the position of the FBGs, they can be classified as central FBGs (contain nine gratings) with an approximate length of 10 mm covering the irradiated area and peripheral FBGs (contain 31 gratings) that measure the temperature of the tissue in the vicinity of the irradiated area. A higher temperature was measured by the FBGs at 808 nm than at 1064 nm, although the difference seems smaller at 6 than at 2 mm. Table II compares the temperature ranges resulting from LA at 808 and 1064 nm. The data were taken at the end of irradiation and after a cooling period of 30 s on the central FBGs. According to the map of the difference in average temperature at a distance of 2 mm, FBGs #15 and #32, which correspond to a sensing length of 20 mm, show a 5%–15% higher temperature when the wavelength is 808 nm. However, at 6 mm, the temperature difference caused by the two wavelengths is insignificant, which is primarily 5% in some regions. Consequently, the pancreatic tissue exhibits approximately comparable thermal response, which can be

TABLE II
COMPARISON OF TEMPERATURE DISTRIBUTION INDUCED BY LA ON CENTRAL FBG SENSORS (10-MM MONITORING LENGTH) AT 808 AND 1064 NM

	Temperature range at the end of irradiation		Temperature range after 30 s cooling	
	2 mm	6 mm	2 mm	6 mm
808 nm	$70 - 96\,°C$	$49 - 59\,°C$	$60 - 71\,°C$	$47 - 53\,°C$
Difference with DPL ($\tau_T = 5\tau_q$)	$5.5 \pm 1\,\%$	$4 \pm 0.5\,\%$	$7 \pm 4\,\%$	$2 \pm 0.5\,\%$
1064 nm	$65 - 89\,°C$	$49 - 56\,°C$	$59 - 72\,°C$	$48 - 53\,°C$
Difference with DPL ($\tau_T = 5\tau_q$)	$6 \pm 2\,\%$	$2 \pm 0.5\,\%$	$7 \pm 3\,\%$	$2 \pm 0.5\,\%$

explained by the close values of effective attenuation coefficients in the pancreatic tissue at the wavelengths of 808 and 1064 nm [18]. The close thermal impact was also observed during the contactless laser irradiation of breast cancer tumor models in mice at 808 and 1064 nm [38]. In another study, the temperature rise recorded by a thermocouple probe in a phantom concentrated with 0.05-nm gold nanostars during laser irradiation at 0.6 W/cm^2 exhibited a comparable increase under both 808- and 1064-nm laser irradiation [39].

Considering that the thermal response of pancreas tissue under light irradiation is only partially investigated because the use of LA for treating pancreatic cancer is at its beginning, the results obtained in this study shed light on several novel aspects. In terms of equipment, we proved that: 1) 808- and 1064-nm laser wavelengths provide a similar overall thermal effect on this tissue from both experimental and numerical viewpoints. This result allows for expanding the range of possible laser sources that could be employed for treating pancreatic cancer and to exploit the combination of LA with other therapies (e.g., nanoparticles-mediated photothermal therapy [15]) and 2) using a diffusing applicator allows to better control the light delivered in the target volume, thus to achieve reproducible experimental results, especially at the margins of the ablated area. The latter are of primary importance for clinicians performing thermal ablations, as the lesion margins allow defining whether a treatment is successful or not [40]. In terms of tissue parameters, we could find the best value of τ_T for the pancreas by comparing the results of the numerical model with the experimental temperature values. This information is of crucial importance for organ-specific therapy planning: it contributes to regulate the heat transfer in the medium and to give information on the optimal laser settings that the clinician can adopt for treating a tumor with a specific size [41], [42].

To leverage the impact of these results on the treatment of pancreatic cancer, future steps should overcome the current experimental limitations, such as the use of an ex vivo model (i.e., absence of blood perfusion and other physiological conditions). Moreover, the numerical model is tuned to the thermal and optical properties of ex vivo pancreas, which have been measured on the same tissue used for the measurements. Thus, additional in vivo studies should be considered in order to take into account the influential physiological conditions and

evaluate the effect of the living pancreas physical properties on the model predictions.

IV. CONCLUSION

This study demonstrates that using the 808- and 1064-nm wavelengths for LA treatment with a diffusing applicator leads to a comparable thermal effect in pancreas. This conclusion was reached owing to the comprehensive temperature distribution monitored by the FBG sensors utilized in the present study. Furthermore, our findings also indicate that incorporating the thermal lagging effect into the pancreas-specific bio-heat transfer model can enhance the accuracy of temperature predictions during LA. Moreover, the temperature data provided by FBGs have been used to optimize some model parameters. As this research has implications for the development of more efficient and effective LA treatment of pancreatic tumor, future in vivo studies, including FBG monitoring of the pancreas thermal response, are expected to consider the influential physiological conditions and their impact on the model predictions.
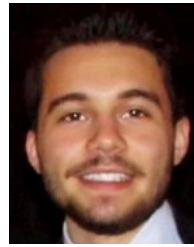
ACKNOWLEDGMENT

REFERENCES

[1] R. L. Siegel, K. D. Miller, H. E. Fuchs, and A. Jemal, "Cancer statistics, 2022," *CA, Cancer J. Clin.*, vol. 72, no. 1, pp. 7–33, Jan. 2022.

[2] M. Orth et al., "Pancreatic ductal adenocarcinoma: Biological hallmarks, current status, and future perspectives of combined modality treatment approaches," *Radiat. Oncol.*, vol. 14, no. 1, pp. 1–20, Dec. 2019.

[3] P. Saccomandi, A. Lapergola, F. Longo, E. Schena, and G. Quero, "Thermal ablation of pancreatic cancer: A systematic literature review of clinical practice and pre-clinical studies," *Int. J. Hyperthermia*, vol. 35, no. 1, pp. 398–418, Dec. 2018.

[4] V. Granata et al., "Assessment of ablation therapy in pancreatic cancer: The radiologist's challenge," *Frontiers Oncol.*, vol. 10, Nov. 2020, Art. no. 560952.

[5] F. M. Di Matteo et al., "Feasibility of EUS-guided Nd:YAG laser ablation of unresectable pancreatic adenocarcinoma," *Gastrointestinal Endoscopy*, vol. 88, no. 1, pp. 168–174, Jul. 2018.

[6] T. A. Jiang, P. Liang, and J. Yu, "Pancreas tumors laser ablation," in *Image-Guided Laser Ablation*, C. M. Pacella, T. A. Jiang, and G. Mauri, Eds. Cham, Switzerland: Springer, 2020, pp. 99–106.

[7] V. G. Truong, S. Jeong, J.-S. Park, S. M. Kim, D. H. Lee, and H. W. Kang, "Endoscopic ultrasound (EUS)-guided cylindrical interstitial laser ablation (CILA) on in vivo porcine pancreas," *Biomed. Opt. Exp.*, vol. 12, no. 7, pp. 4423–4437, 2021.

[8] A. J. Welch and M. J. C. Van Gemert, Eds., *Optical-Thermal Response of Laser-Irradiated Tissue*, vol. 2. New York, NY, USA: Springer, 2011.

[9] F. Di Matteo et al., "U.S.-guided application of Nd:YAG laser in porcine pancreatic tissue: An ex vivo study and numerical simulation," *Gastrointestinal Endoscopy*, vol. 78, no. 5, pp. 750–755, 2013.

[10] S. Lim et al., "Endoscopic ultrasound-guided laser ablation using a diffusing applicator for locally advanced pancreatic cancer treatment," *Cancers*, vol. 14, no. 9, p. 2274, May 2022.

[11] J. Lee et al., "Endoscopic ultrasound-guided pancreatic interstitial laser ablation using a cylindrical laser diffuser: A long-term follow-up study," *Biomedicines*, vol. 10, no. 11, p. 2895, Nov. 2022.

[12] T. H. Nguyen, S. Park, K. K. Hlaing, and H. W. Kang, "Temperature feedback-controlled photothermal treatment with diffusing applicator: Theoretical and experimental evaluations," *Biomed. Opt. Exp.*, vol. 7, no. 5, pp. 1932–1947, 2016.

[13] F. Morra et al., "Spatially resolved thermometry during laser ablation in tissues: Distributed and quasi-distributed fiber optic-based sensing," *Opt. Fiber Technol.*, vol. 58, Sep. 2020, Art. no. 102295.

[14] P. Saccomandi et al., "Theoretical analysis and experimental evaluation of laser-induced interstitial thermotherapy in ex vivo porcine pancreas," *IEEE Trans. Biomed. Eng.*, vol. 59, no. 10, pp. 2958–2964, Oct. 2012.

[15] L. Bianchi et al., "Fiber Bragg grating sensors-based thermometry of gold nanorod-enhanced photothermal therapy in tumor model," *IEEE Sensors J.*, vol. 22, no. 12, pp. 11297–11306, Jun. 2022.

[16] P. Gupta and A. Srivastava, "Non-Fourier transient thermal analysis of biological tissue phantoms subjected to high intensity focused ultrasound," *Int. J. Heat Mass Transf.*, vol. 136, pp. 1052–1063, Jun. 2019.

[17] T.-C. Shih, H.-S. Kou, C.-T. Liauh, and W.-L. Lin, "The impact of thermal wave characteristics on thermal dose distribution during thermal therapy: A numerical study," *Med. Phys.*, vol. 32, no. 9, pp. 3029–3036, Aug. 2005.

[18] P. Lanka, L. Bianchi, A. Farina, M. De Landro, A. Pifferi, and P. Saccomandi, "Estimation of porcine pancreas optical properties in the 600–1100 nm wavelength range for light-based therapies," *Sci. Rep.*, vol. 12, no. 1, p. 14300, Aug. 2022.

[19] B. Kaur, S. Kumar, and B. K. Kaushik, "2D materials-based fiber optic SPR biosensor for cancer detection at 1550 nm," *IEEE Sensors J.*, vol. 21, no. 21, pp. 23957–23964, Nov. 2021.

[20] S. Kumar et al., "Plasmon-based tapered-in-tapered fiber structure for p-cresol detection: From human healthcare to aquaculture application," *IEEE Sensors J.*, vol. 22, no. 19, pp. 18493–18500, Oct. 2022.

[21] S. Korganbayev et al., "PID controlling approach based on FBG array measurements for laser ablation of pancreatic tissues," *IEEE Trans. Instrum. Meas.*, vol. 70, pp. 1–9, 2021.

[22] A. V. Dostovalov, A. A. Wolf, A. V. Parygin, V. E. Zyubin, and S. A. Babin, "Femtosecond point-by-point inscription of Bragg gratings by drawing a coated fiber through ferrule," *Opt. Exp.*, vol. 24, no. 15, pp. 16232–16237, 2016.

[23] L. Huang, R. S. Dyer, R. J. Lago, A. A. Stolov, and J. Li, "Mechanical properties of polyimide coated optical fibers at elevated temperatures," *Proc. SPIE*, vol. 9702, pp. 177–184, Mar. 2016.

[24] L. Bianchi, S. Korganbayev, A. Orrico, M. De Landro, and P. Saccomandi, "Quasi-distributed fiber optic sensor-based control system for interstitial laser ablation of tissue: Theoretical and experimental investigations," *Biomed. Opt. Exp.*, vol. 12, no. 5, pp. 2841–2858, 2021.

[25] Y. Zhang, "Generalized dual-phase lag bioheat equations based on nonequilibrium heat transfer in living biological tissues," *Int. J. Heat Mass Transf.*, vol. 52, nos. 21–22, pp. 4829–4834, Oct. 2009.

[26] J. Zhou, Y. Zhang, and J. K. Chen, "An axisymmetric dual-phase-lag bioheat model for laser heating of living tissues," *Int. J. Thermal Sci.*, vol. 48, no. 8, pp. 1477–1485, Aug. 2009.

[27] P. Namakshenas and A. Mojra, "Efficient drug delivery to hypoxic tumors using thermosensitive liposomes with encapsulated anti-cancer drug under high intensity pulsed ultrasound," *Int. J. Mech. Sci.*, vol. 237, Jan. 2023, Art. no. 107818.

[28] K. Mitra, S. Kumar, A. Vedevarz, and M. K. Moallemi, "Experimental evidence of hyperbolic heat conduction in processed meat," *J. Heat Transf.*, vol. 117, no. 3, pp. 568–573, Aug. 1995.

[29] W. Roetzel, N. Putra, and S. K. Das, "Experiment and analysis for non-Fourier conduction in materials with non-homogeneous inner structure," *Int. J. Thermal Sci.*, vol. 42, no. 6, pp. 541–552, Jun. 2003.

[30] I. Eltejaei, M. Balavand, and A. Mojra, "Numerical analysis of non-Fourier thermal response of lung tissue based on experimental data with application in laser therapy," *Comput. Methods Programs Biomed.*, vol. 199, Feb. 2021, Art. no. 105905.

[31] C. Li et al., "Fourier and non-Fourier bio-heat transfer models to predict ex vivo temperature response to focused ultrasound heating," *J. Appl. Phys.*, vol. 123, no. 17, May 2018, Art. no. 174906.

[32] P. Namakshenas and A. Mojra, "Optimization of polyethylene glycol-based hydrogel rectal spacer for focal laser ablation of prostate peripheral zone tumor," *Phys. Medica*, vol. 89, pp. 104–113, Sep. 2021.

[33] D. Yang, M. C. Converse, D. M. Mahvi, and J. G. Webster, "Measurement and analysis of tissue temperature during microwave liver ablation," *IEEE Trans. Biomed. Eng.*, vol. 54, no. 1, pp. 150–155, Jan. 2007.

[34] A. Mohammadi, L. Bianchi, S. Asadi, and P. Saccomandi, "Measurement of ex vivo liver, brain and pancreas thermal properties as function of temperature," *Sensors*, vol. 21, no. 12, p. 4236, Jun. 2021.

[35] J. Schaible et al., "Safety margin assessment after microwave ablation of liver tumors: Inter- and intrareader variability," *Radiol. Oncol.*, vol. 54, no. 1, pp. 57–61, Feb. 2020.

[36] K. F. Chu and D. E. Dupuy, "Thermal ablation of tumours: Biological mechanisms and advances in therapy," *Nature Rev. Cancer*, vol. 14, no. 3, pp. 199–208, Mar. 2014.

[37] V. Lopresto, R. Pinto, L. Farina, and M. Cavagnaro, "Treatment planning in microwave thermal ablation: Clinical gaps and recent research advances," *Int. J. Hyperthermia*, vol. 33, no. 1, pp. 83–100, Jan. 2017.

[38] L. Bianchi et al., "Thermal analysis of laser irradiation-gold nanorod combinations at 808 nm, 940 nm, 975 nm and 1064 nm wavelengths in breast cancer model," *Int. J. Hyperthermia*, vol. 38, no. 1, pp. 1099–1110, Jan. 2021.

[39] Y. Liu et al., "Plasmonic gold nanostars for synergistic photoimmunotherapy to treat cancer," *Nanophotonics*, vol. 10, no. 12, pp. 3295–3302, Sep. 2021.

[40] A.-M. Pausch et al., "Stereotactic microwave ablation of hepatocellular carcinoma: The impact of tumor size and minimal ablative margin on therapeutic success," *Tomography*, vol. 9, no. 1, pp. 50–59, Dec. 2022.

[41] K.-C. Liu and T.-M. Chen, "Comparative study of heat transfer and thermal damage assessment models for hyperthermia treatment," *J. Thermal Biol.*, vol. 98, May 2021, Art. no. 102907.

[42] C. Li, S. Chen, Q. Wang, H. Li, S. Xiao, and F. Li, "Effects of thermal relaxation on temperature elevation in ex vivo tissues during high intensity focused ultrasound," *IEEE Access*, vol. 8, pp. 212013–212021, 2020.

Leonardo Bianchi (Member, IEEE) received the M.Sc. (cum laude) degree in biomedical engineering and the Ph.D. (cum laude) degree in mechanical engineering with the European Doctoral Title from the Politecnico di Milano, Milan, Italy, in 2019 and 2023, respectively. He is currently working as a Postdoctoral Research Fellow in the framework of the European Research Council (ERC)-funded LASER OPTIMAL project (Laser Ablation: SElectivity and monitoRing for OPTImal tuMor removAL), Politecnico di Milano. His research interests include the optimization of laser ablation of tumors, from both numerical modeling and experimental assessment, nanoparticle-assisted photothermal therapies, and the related sensing techniques for temperature monitoring during treatments.

Pouya Namakshenas received the M.Sc. degree in mechanical engineering-energy conversion from K. N. Toosi University, Tehran, Iran, in 2020.

He joined the Department of Mechanical Engineering, Politecnico di Milano, Milan, Italy, as a Researcher to work on the last phase of LASER OPTIMAL project (European Research Council Grant). As part of his role, he is developing a computational model to optimize laser interstitial thermotherapy for the ablation of pancreatic tumors. His research has been mainly dedicated to in silico oncology, particularly in the areas of hyperthermia therapy, and targeted drug delivery systems.

Paola Saccomandi (Senior Member, IEEE) received the Ph.D. degree in biomedical engineering from the Università Campus Bio-Medico di Rome, Rome, Italy, in 2014.

From 2016 to 2018, she was a Postdoctoral Researcher with the IHU Strasbourg—Institute of Image-Guided Surgery of Strasbourg, Strasbourg, France. Since 2018, she has been an Associate Professor with the Department of Mechanical Engineering, Politecnico di Milano, Milan, Italy. She is the Principal Investigator of European Research Council Grants and national projects. Her main research interests include fiber optic sensors and measurement systems for thermal, mechanical, and biomedical measurements, biomedical imaging, and the development of light-based approaches for hyperthermal tumor treatment and monitoring.